applied optics

Estimation of the GSSM calibration error

LINCHU HAN,[1,2,*] JINGXU ZHANG,[1] FEI YANG,[1] AND QICHANG AN[1,2]

[1]Changchun Institute of Optics, Fine Mechanics and Physics, Chinese Academy of Sciences, Changchun 130033, China
[2]University of Chinese Academy of Sciences, Beijing 100039, China
*Corresponding author: hlc2201@hotmail.com

Received 1 July 2016; revised 5 September 2016; accepted 27 September 2016; posted 30 September 2016 (Doc. ID 269717); published 28 October 2016

The calibration of the tertiary mirror of the Thirty Meter Telescope, also known as the giant science steering mirror (GSSM), is a step of great significance during its testing process. Systematic, drift, and random errors constitute the major limitations to the accuracy of the calibration measurements. In this article, we estimated the errors in the calibration of the GSSM with a laser tracker. For the systematic error, a measurement strategy based on the standard bar method was successfully designed and applied. At the same time, we can distinguish between the drift and random errors by means of a correlation analysis. The systematic error, which depends strongly on the configuration of the system formed by the GSSM and the laser tracker, was estimated to be 20 μm for the GSSM prototype. The random error, averaging 15 min, was about 4 μm. The correlation coefficients among three different noise measurements are all lower than 0.1, which indicates that the noise is dominated by random errors. Finally, the error can be sufficiently suppressed by rearranging the position of the spherically mounted retroreflectors. The result shows that the accuracy of the measurement can be improved by 21.4% with the new arrangement method.

OCIS codes: (110.6770) Telescopes; (120.0120) Instrumentation, measurement, and metrology; (150.1488) Calibration; (220.4840) Testing; (140.3490) Lasers, distributed-feedback.

http://dx.doi.org/10.1364/AO.55.008884

1. INTRODUCTION

The Thirty Meter Telescope (TMT) will be one of the largest telescopes in the world. It will be equipped with active optics and an extremely large segmented main mirror, which will provide the telescope with a dramatically increased light collection capability. The tertiary mirror (M3) of the TMT, also known as the giant steering science mirror (GSSM), will reflect light to the Nasmyth platform. The CIOMP (Changchun Institute of Optics, Fine Mechanics, and Physics) is in charge of constructing the GSSM. In order to understand its requirements and characteristic errors, the CIOMP decided to build a 1/4-scale prototype, the so-called GSSMP [1–3].

The GSSM will be responsible for the pointing, slewing, tracking, and guiding operations. Pointing is a blind operation that aligns the telescope to targets in the sky with no optical feedback; this alignment will be controlled by the instruments on the Nasmyth Platform via rotation and tilting axes of the GSSM. Slewing can be described as a fast movement of the GSSM between two positions. Tracking involves smoothly following the target. Finally, guiding stands for closed-loop tracking with optical feedback. Tracking and guiding will be under the command of the control system. Because of the long distance traveled by the transmitted light, the GSSM relies on accurate calibration of the tertiary mirror to achieve the required precision in the pointing process [4–6].

The GSSM calibration aims to minimize the error between a commanded rotated position (registered by encoders) and the actual rotated position (measured with a laser tracker) [7–9]. Hence, it involves two different steps: the calibration of the encoders and that of the laser tracker. The tertiary mirror is so large that it works in very complicated load conditions (at most 90° degrees off the zenith). Besides, the light reflection ability of the GSSM is very sensitive to the rigid-body displacement of the mirror. Although traditional calibration instruments (autocollimator, for instance) can meet the accuracy requirements for the measurement, they do not allow changing the orientation of the measurement. A laser tracker not only provides high measuring accuracy but also is able to realize rotation and elevation. It can measure both the distance between objects and the deflection angles in the horizontal and vertical directions by using a distance-measuring interferometer and two angular encoders [10].

Nevertheless, with the increase of optical element diameter, the measuring area of the laser tracker also becomes larger, which as a result, leads to the loss of measuring accuracy. Based on the double frequency laser interference technique, the distance measuring precision of the laser tracker can still reach submicron level on a large scale [11]. However, affected by type, structure, and installation of encoders, the angle measuring precision is comparably lower, which makes it the main source of error of the laser tracker. Therefore, the angle measuring accuracy of the laser tracker must be further improved before calibrating the GSSM.

Angle measurement by laser tracker has been studied by scholars. Lin improved the accuracy to several arcsec by moving a laser tracker to different stations [12]. Ma used a laser tracker to evaluate the error in small angular motion (1 deg at maximum) [13]. The mentioned methods both used one spherically mounted retroreflector (SMR). Wang proposed a self-calibration method, regarded as the iterative process of the equal division average method (EDA-method), which used three or four SMRs for higher accuracy [14]. Due to the limited space and the extremely large travel range of the GSSM, the first two methods cannot meet the requirements. As for the EDA-method, the way of multiple angle measuring components is practical and effective. However, the arrangement of SMRs can be further optimized to improve the accuracy of angle measurement [15].

In this paper, first the error source of the laser tracker is analyzed from three aspects: systematic, drift, and random errors. Second, by rearranging the position of the SMRs, an error suppression method is proposed to improve the accuracy of the angle measurement. Finally, the numerical simulation and experiment are conducted to improve the effectiveness of the error analysis and suppression method.

2. DEFINITIONS AND ANALYSIS

A. Definition of the GSSMP Coordinate System

The first thing that needs to be defined is the coordinate system of the tertiary mirror. All motions are about the Z-axis of the elevation coordinate system (ECRS) and the X-axis of the M3 coordinate system (M3CRS). For the calibration, the goal is to precisely measure the difference between commanded and actual positions and then to fine-tune the performance by means of control algorithms. In order to measure the actual position and check that all the motion requirements are fulfilled [16], a calibration lookup table that lists encoder readings was created.

The support interface (black one under the SMR) shown in the small interface in Fig. 1 is screwed to the GSSMP. It is more convenient to place the SMRs in different places of the GSSMP. The repeatability accuracy of this system is also very good (less than 10 μm). The experiment was carried out in the laboratory, with a room temperature of 24.3°C. SMRs will be located on the yoke. The line between the two targets will define the M3CRS X-axis. By rotating the positioner, the ECRS Z-axis can also be defined.

B. Error Analysis for the Laser Tracker Measurement

Before the calibration, an error analysis was performed to analyze the sources of error for the laser tracker and try to minimize this error. A correct calibration of the laser tracker is essential because its accuracy is the major limiting factor in the calibration of the mirror. Measurement errors can be divided in three types: systematic, drift, and random error [17–19].

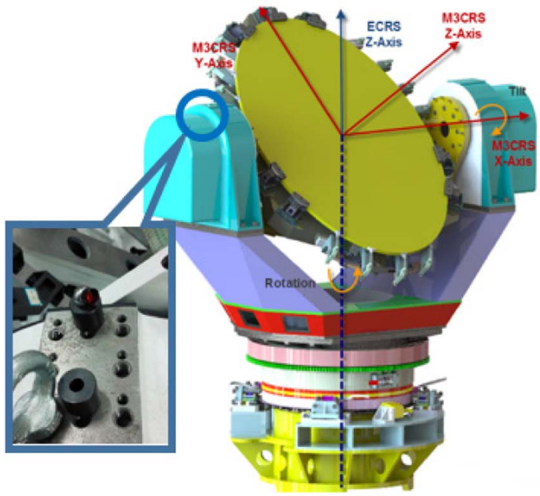

Fig. 1. GSSM mirror, showing details of the assembly and the two relevant coordinate systems for the TMT M3.

Systematic errors are characterized by low spatial and temporal frequency and can be partially suppressed by using the lookup table. On the other hand, random errors can be minimized through averaging. Finally, drift errors are those whose characteristic time is comparable to the duration of the test. Therefore, drift errors force us to limit the measurement duration.

In this study, the three types of error were estimated and compared to the GSSM/GSSMP requirements, choosing the best testing approach.

1. Systematic Error Analysis

The laser tracker can define the coordinates of the SMR. Therefore, the angle can be obtained by using the basic sine or cosine laws for triangles. The angular testing performed with the laser tracker is based on the formula

$$\theta = 2 \text{ arc sin}\left(\frac{\Delta}{2r}\right), \quad (1)$$

where θ is the angle that we want to measure, Δ is the displacement realized by the laser tracker, and r is the rotational radius of the SMR, as shown in the left panel of Fig. 2. The error in the angle can be expressed as

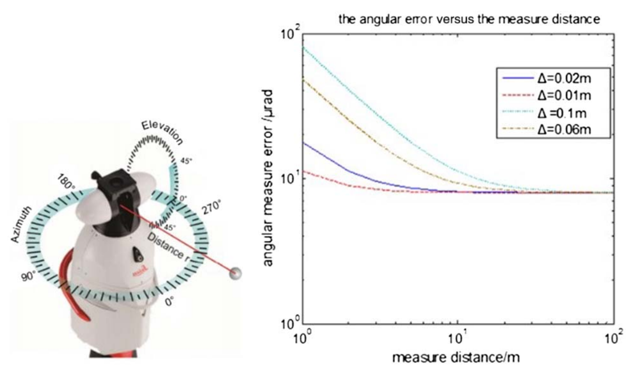

Fig. 2. Laser tracker angular error.

$$\delta\theta = \frac{\sqrt{\left(\frac{\delta\Delta}{r}\right)^2 + \left(\frac{\delta r\Delta}{r^2}\right)^2}}{\cos\left(\frac{\theta}{2}\right)}, \tag{2}$$

where $\delta\Delta$ is the error of the angle measurement. $\delta\Delta$ is in the position measurement, and δr is the location error along the laser beam. According to the specifications provided by the vendor, $\delta\Delta = \delta r = \alpha r$(where we chose $\alpha = 8\ \mu\text{m/m}$ provided by the vendor). $\delta\theta$ is shown in Fig. 2, where the angular accuracy is limited by the value of α, a theoretical limit for accuracy calibration. Under this limitation, enlarging the testing radius can increase the angular precision.

While the error of the laser tracker in a certain testing configuration can be simulated using a Monte Carlo method, such a simulation cannot always fill the gap between the actual system (the GSSM/GSSMP in our case) and the theoretical model. First and foremost, the theoretical model cannot account for the spatial limitations of the laser beam. Unfortunately, Monte Carlo methods assume that all the data points used in the simulation will be tested in the practical measurement. This is the main reason to opt for practical error testing instead. Furthermore, the conditions in the testing facility (temperature, environmental vibrations, etc.) are complicated and impossible to predict. Hence, the simulation is not capable of taking all of these factors into consideration. Though the laser tracker can compensate for the turbulence of the air only partially, it is better to do the error estimation by practical testing [20].

Practical error estimation was realized by testing the length of a standard alloy bar. This allows measuring the accuracy of the laser tracker at a certain position. In order to prevent the error accumulation characteristic of laser tracker systems, it is necessary to minimize the duration of the test and the changes in the position of the laser tracker itself. Therefore, the standard bar was set vertically to the line between the laser tracker and the center of the standard bar, which is as close as possible to the GSSM/GSSMP. The experimental setup for the calibration is shown in Fig. 3.

Fig. 3. Experimental setup for the error calibration of the laser tracker.

The length of the standard bar (which was 1016.0151 mm) was measured previously by the CMM with an accuracy of 3 μm. The measurement by the laser tracker was performed as follows (see Fig. 4): we placed the bar at location #1 and recorded the coordinates of point B2; then we measured ten times the length $\overline{B1B3}$ and calculated the average; finally, we placed the bar at locations #2–#4 and repeated the previous steps. The values of $\overline{B1B3}$ measured at the different positions are displayed in Fig. 4. The average location accuracy is 20 μm.

The angular accuracy for the tilt axis can be calculated using the following formula:

$$\Delta\theta_{\text{tilt}} = \frac{\Delta r}{r}, \tag{3}$$

where $\Delta\theta_{\text{tilt}}$ is the angular accuracy, Δr is the location accuracy, and r is the rotational radius of the SMR at locations #1 and #3. Figure 5 shows the geometry and dimensions of the GSSM. The lengths of the major and minor axes are 1797 mm and 1288 mm, respectively, whereas the corresponding values for

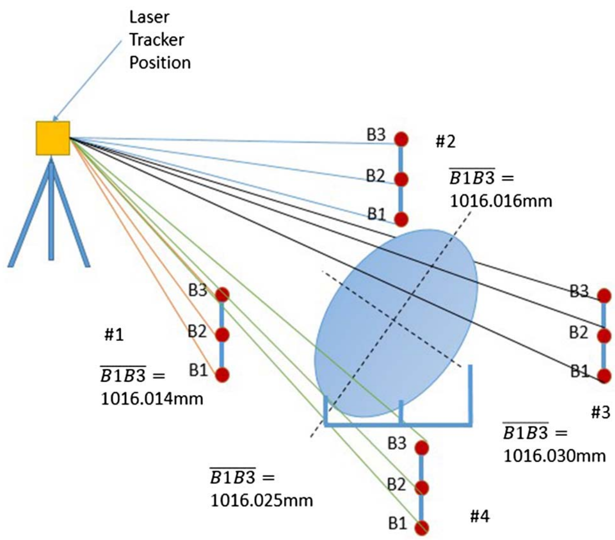

Fig. 4. Measurement of the systematic error of the laser tracker.

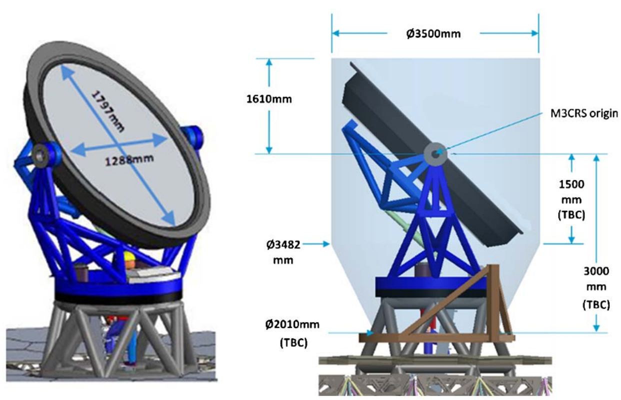

Fig. 5. Geometry and dimensions of the GSSM.

the prototype are 447 and 327 mm. When the GSSM rotates around the rotation axis, r is the major axis, while if the GSSM rotates around the tilt axis, r is the minor axis. Thus, the systematic measurement error for the tilt axis is

$$\Delta\theta_{\text{tilt}} = \frac{20\ \mu\text{m}}{447\ \text{mm}} = 9.2''.$$

The angular accuracy for the rotation axis can be calculated through

$$\Delta\theta_{\text{rotate}} = \frac{\Delta r}{r}, \tag{4}$$

where $\Delta\theta_{\text{rotate}}$ is the angular accuracy, Δr is the average location accuracy, and r is the rotational radius of the SMR at locations #2 and #4. The systematic measurement error for the rotation axis is

$$\Delta\theta_{\text{rotate}} = \frac{20\ \mu\text{m}}{327\ \text{mm}} = 12.6''.$$

According to the design requirement [REQ-2-M3-0920], the M3 system (M3S) shall be able to rotate the M3 mirror about the ECRS Z-axis to any angle within the range with a repeatable residual M3 rotation error (after telescope calibration) that is less than 3.5 arcsec RMS. According to our results,

$$\Delta\theta_{\text{tilt}} = \frac{20\ \mu\text{m}}{1797\ \text{mm}} = 2.2''.$$

According to the requirement [REQ-2-M3-0930], the M3S should be able to tilt the M3 mirror about the M3CRS X-axis to any angle within the range with a repeatable residual M3 tilt error (after telescope calibration) that is less than 3.5 arcsec RMS [21]. We find that

$$\Delta\theta_{\text{rotate}} = \frac{20\ \mu\text{m}}{1288\ \text{mm}} = 3.2''.$$

Hence, the GSSM will meet both requirements.

2. *Drift Error Analysis*

Drift errors are the errors between systematic errors and random errors, which have characteristic durations shorter than systematic errors (the latter are considered not to change during measurement). On the other hand, the characteristic duration is longer for drift errors than for random errors (random errors are related to neither time nor other data).

The drift error E_d can be expanded as a MacLaurin series in time t as

$$E_d = \sum_{i=0}^{\infty} \frac{E_d^{(n)}}{i!} t^i. \tag{5}$$

We assume the drift error follows a quadratic law of t, so it can be expressed as

$$E_d = \alpha + \beta t + \gamma t^2. \tag{6}$$

The correlation coefficient of different sampling lengths has the following form:

$$C(x, y) = \frac{\sum (x_i - E_x)(y_i - E_y)}{D_x D_y}. \tag{7}$$

where x_i and y_i are the data, E_x and E_y are the estimated values for x_i and y_i, and D_x and D_y are the standard deviations of x_i and y_i, respectively. If two rows of data have drift errors $E_{d1} = \alpha_1 + \beta_1 t$ and $E_{d2} = \alpha_2 + \beta_2 t$, the correlation coefficient is

$$C(E_{d1}, E_{d2}) = 1.$$

The drift error is always strongly coupled with the random error, so they will be tested together and analyzed using the correlation coefficient in the next section.

3. *Random Error Analysis*

The random error can be partially suppressed by averaging over multiple measurements. However, unless the number of measurements is sufficiently large, the random error will still play a role in the testing results.

The correlation coefficient can direct the judgment of random error. If the random noise is truly "random," the correlation coefficient will be very small. At the same time, using the correlation analysis, the drift error and the random error can be told. Compared to the drift error, the correlation coefficient of random error will be significantly larger, whence the correlation coefficient can serve to recognize the random error. Here, we recorded the error of the laser tracker at different times, places, and temperatures.

As the drift error depends strongly on the duration of the measurement, we completed all the tests at each position in 15 min position. We followed these steps:

1. Set the laser tracker pointing to a certain position and record its reading for 15 min.
2. Then direct the laser tracker to another position and do the same.
3. If the two datasets present a large correlation, it means the data are affected by drift errors. Otherwise, if there is no relationship between the two datasets that means the error is just random.
4. For the drift error, we should perform a quadratic fit to extract the drifting term, whereas the random error can be suppressed by averaging multiple measurements.

The measured signals are shown in Fig. 6. As previously commented, the three series of data correspond to different locations and conditions, such as temperature and air turbulence. The correlation coefficient matrix is represented graphically Fig. 7. The self-correlation coefficients are obviously

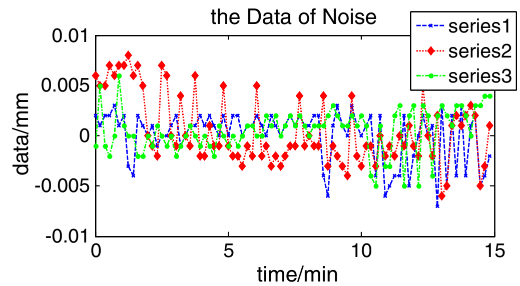

Fig. 6. Measurement of the random error of the laser tracker.

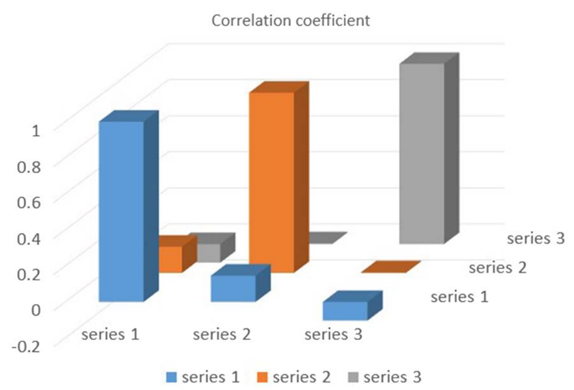

Fig. 7. Calculation of the correlation coefficient between the different measurements of the error of the laser tracker.

one, while the cross-correlation coefficients are 0.14, 0.06, and 0.001. This means that the noise is more likely due to the random error rather than the drift error during the 15 min measurements.

The magnitude of the random error is about 0.003 mm. Due to the averaging effect, the random error is much smaller than the systematic error.

We were careful to perform the measurements in a moment of small temperature variation since such a change would affect the results. For the GSSMP testing, the calibration will be processed after the temperature is tested in previous days.

3. ERROR SUPPRESSION

In the previous section, we analyzed the error through one-point measurements. However, calibration is essentially an angle-testing procedure, whose accuracy will be strongly influenced by the location of sensors and the algorithm used to process the raw data.

Angle has a peculiarity that it is a 360° closed system [22–24]. The equal-weights error $\Delta\theta$ can be expressed as a Fourier series with components of different orders. The following expression includes most of the systematic and random errors:

$$\Delta\theta = \sum_{k=1}^{m} \frac{e_k}{R} \sin(k\theta), \tag{8}$$

where $k = 1 \cdots m$ is the order of the Fourier harmonic representing the amplitude of the spatial frequency error, θ is the angle covered by the system, e_k is the magnitude of the k order error, and R is the radius of gyration. If the angle measurement error is achieved by performing N readings with equal intervals, the readout $\Delta\theta_\Sigma$ can be expressed as

$$\Delta\theta_\Sigma = \frac{1}{N}\sum_{k=1}^{m}\frac{e_k}{R}\left\{\begin{array}{l}\sin(k\theta) + \sin\left(k\theta + k\frac{2\pi}{N}\right) + \cdots \\ + \sin\left[k\theta + k(N-1)\frac{2\pi}{N}\right]\end{array}\right\}. \tag{9}$$

We can reformulate this equation using a basic trigonometric relationship:

$$\begin{aligned}\Delta\theta_\Sigma &= \frac{1}{N}\sum_{k=1}^{m}\frac{e_k}{R}\left\{\sin(k\theta) + \sin(k\theta)\cos\left(k\frac{2\pi}{N}\right)\right.\\
&\quad + \cos(k\theta)\sin\left(k\frac{2\pi}{N}\right) + \cdots + \sin(k\theta)\cos\left[k(N-1)\frac{2\pi}{N}\right]\\
&\quad \left. + \cos(k\theta)\sin\left[k(N-1)\frac{2\pi}{N}\right]\right\}\\
&= \frac{1}{N}\sum_{k=1}^{m}\frac{e_k}{R}\left\{\sin(k\theta) + \sin(k\theta)\cos\left(k\frac{2\pi}{N}\right)\right.\\
&\quad + \cos(k\theta)\sin\left(k\frac{2\pi}{N}\right) + \cdots + \sin(k\theta)\cos\left[k(N-1)\frac{2\pi}{N}\right]\\
&\quad \left. + \cos(k\theta)\sin\left[k(N-1)\frac{2\pi}{N}\right]\right\}\\
&= \frac{1}{N}\sum_{k=1}^{m}\frac{e_k}{R}\left\{\sin(k\theta) + \sin(k\theta)\cos\left(k\frac{2\pi}{N}\right) + \cdots\right.\\
&\quad \left. + \sin(k\theta)\cos\left[k(N-1)\frac{2\pi}{N}\right]\right\}\\
&\quad + \frac{1}{N}\sum_{k=1}^{m}\frac{e_k}{R}\left\{\cos(k\theta)\sin\left(k\frac{2\pi}{N}\right) + \cdots\right.\\
&\quad \left. + \cos(k\theta)\sin\left[k(N-1)\frac{2\pi}{N}\right]\right\}.\end{aligned} \tag{10}$$

Then, after the calculation, we get the following estimation in short. The following Eq. (11) can indicate the relationship between readout error and the number of the reading heads:

$$\Delta\theta_\Sigma = \frac{1}{N}\frac{e_k}{R}\left[\frac{\cos\left[k(N-1)\frac{\pi}{N}\sin\left(Nk\frac{\pi}{N}\right)\right]}{\sin\left(k\frac{\pi}{N}\right)}\right]. \tag{11}$$

Assuming that $k = cN$ (where c is an integer), we obtain the magnitude of the read out error as

$$|\Delta\theta_\Sigma| = \frac{e_k}{R}. \tag{12}$$

On the other hand, if $k \neq cN$, then $|\Delta\theta_\Sigma| = 0$. Therefore, only the error components with $k \neq cN$ can be suppressed. It is obvious that $c \geq 2$, so the error involving the decenter of the sensor will be suppressed. Thus, the location accuracy of the SMR will also loose. In other words, calibration is not affected by the mechanical error involved by the nest itself.

The original location of the SMR for the calibration is shown in Fig. 8. Figure 8(a) presents the configuration used for the rotation axis and Fig. 8(b) shows that employed for the tilt axis.

For rotation, the SMR 2, 4 shall be located at the peaks of an equilateral triangle and 1, 3 be located at the opposite peaks of the diameter. The equal-weights error can be expressed as

$$\theta_{\text{rotation}} = \frac{1}{4}(T_1 + T_2 + T_3 + T_4), \tag{13}$$

where θ_{rotation} is the rotation angle under testing, and $T_1 - T_4$ are the corresponding angular changes of the SMR 1–4.

By Eq. (9), the error of the rotation angle measurement in which accuracy is equal to the two-reading-heads case can be

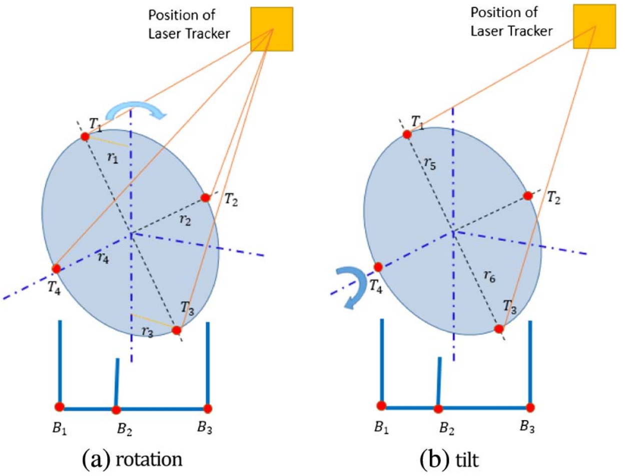

Fig. 8. Configuration of the calibration with a laser tracker for (a) the rotation axis and (b) the tilt axis.

expressed as the following equation, where $r_1 = r_3 = R_1$, $r_2 = r_4 = R_2$, and $N = 2$:

$$\Delta\theta_\Sigma = \frac{1}{2}\sum_{k=1}^{m}\frac{e_k}{R_1}\left\{\sin(k\theta) + \sin\left(k\theta + 3k\frac{2\pi}{N}\right)\right\} + \frac{1}{2}\sum_{k=1}^{m}\frac{e_k}{R_2}\left\{\sin\left(k\theta + 2k\frac{2\pi}{N}\right) + \cdots + \sin\left(k\theta + 4k\frac{2\pi}{N}\right)\right\}. \quad \textbf{(14)}$$

To improve the measurement accuracy, we chose the weights as here we chose the weights as $\frac{R_2}{R_1+R_2}$ for the test points T_1, T_3 and $\frac{R_1}{R_1+R_2}$ for the points T_2, T_4:

$$\theta_{\text{rotation}} = \frac{1}{2}\frac{R_2}{R_1 + R_2}(T_1 + T_3) + \frac{1}{2}\frac{R_1}{R_1 + R_2}(T_2 + T_4). \quad \textbf{(15)}$$

Using those weights, the error can be expressed as the following Eq. (16), where $r_1 = r_3 = R_1$, $r_2 = r_4 = R_2$, and $N = 2$:

$$\begin{aligned}\Delta\theta_\Sigma &= \frac{1}{2}\frac{R_1}{R_1+R_2}\sum_{k=1}^{m}\frac{e_k}{R_1}\left\{\sin(k\theta) + \sin\left(k\theta + 3k\frac{2\pi}{N}\right)\right\} \\ &\quad + \frac{1}{2}\frac{R_2}{R_1+R_2}\sum_{k=1}^{m}\frac{e_k}{R_2}\left\{\sin\left(k\theta + 2k\frac{2\pi}{N}\right) + \sin\left(k\theta + 4k\frac{2\pi}{N}\right)\right\} \\ &= \frac{1}{2}\frac{1}{R_1+R_2}\sum_{k=1}^{m}e_k\left\{\sin(k\theta) + \sin\left(k\theta + 2k\frac{2\pi}{N}\right)\right. \\ &\quad \left. + \sin\left(k\theta + 3k\frac{2\pi}{N}\right) + \sin\left(k\theta + 4k\frac{2\pi}{N}\right)\right\}. \quad \textbf{(16)}\end{aligned}$$

It is in accordance with the four SMRs case. The error components except for the $4 \times c$ order will be suppressed.

For the tilt, T_2, T_4 are not available for the calculation. Hence, the accuracy is equal to the two reading head average case. All components except those of $2 \times c$ order can be suppressed. By the weighted method, the accuracy of the rotation angle can be improved. Due to the limited space, it can be measured only by two SMRs.

We ran a simulation to verify the error suppression procedure. We provide four deviation series, which are shifted by $\frac{\pi}{2}$ and added some amount of noise, as shown in Fig. 9.

The error can be minimized through averaging. The error series before and after averaging are shown in Fig. 10. We can see that the error has been obviously constrained.

The Fourier components of the error before and after averaging are shown in Fig. 11. All components except those whose order is a multiple of four get suppressed. While the error originally contains all the components, after averaging it contains only those with order 4, 8, 12, 16, and 20. At the same time,

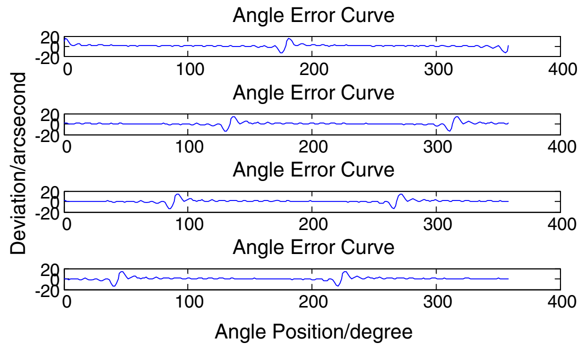

Fig. 9. Four series of angle error data, shifted by $\frac{\pi}{2}$.

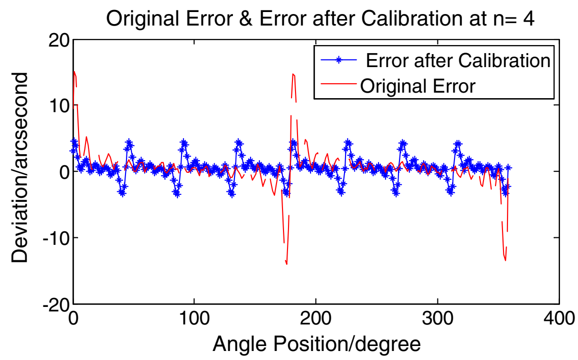

Fig. 10. Error before and after averaging.

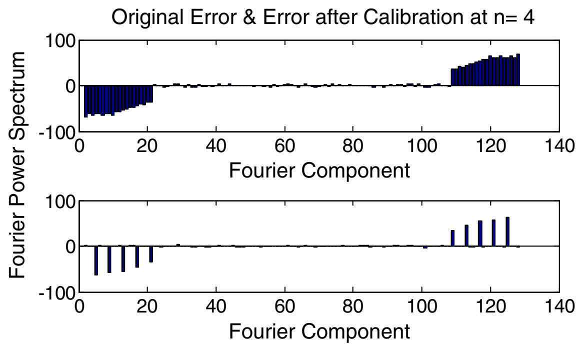

Fig. 11. Fourier components of the error before and after averaging.

random errors with large temporal frequency are suppressed due to the averaging.

According to the previous analysis, the SMR should be located with equal interval. By the utilization of 4 SMRs, all components except those with order $4 \times c$ will be suppressed.

The existing method of error measurement and suppression for the laser tracker can be summarized. The early research mainly used one reading head for measurement. In order to improve the accuracy of the angle encoder, multireading heads and the Fourier components distribution of the angle encoder deviation also have been discussed by other scholars. However, the accuracy can be further improved if we use a certain quantity of SMRs. If that number is 4, it can be expressed as $4 = 3 + 2 - 1$. Thus, we can divide the SMRs in two groups of 3 and 2 SMRs, whence all components of the error except those with order $3 \times 2 \times c$ will be suppressed. Thus, we can rearrange the SMR assignment. The quantity of the SMRs is the same, but the four SMRs can be expressed as the combination of a line and a triangle. This configuration is shown in Fig. 12.

We consider four deviation series, where three of which are shifted by $\frac{2\pi}{3}$ and two are shifted by π. The error series before and after averaging are shown in Fig. 13. We can see that the error is obviously suppressed by performing the average. All components of the error except those whose order is a multiple of 6 get suppressed, as shown in Fig. 14, resulting in an error much smaller than in the case when $n = 4$.

Based on the previous analysis, the SMRs can be rearranged. There are still 4 SMRs on the GSSMP dummy mirror. To ensure the same rotational radius, the location is carefully calculated.

It is difficult to have SMRs at T_2 or T_4 due to the limited space left by the yoke. If the SMR T_2, T_4 could be located like in Fig. 15, there would be more space left. Hence, such a configuration would be more convenient to perform the metrology. The configuration of the testing plan for both tilt and rotation is shown in Fig. 15. SMR $T_1 - T_4$ has the same radius for rotation and for tilt, but it has two kinds of length. All error components will be suppressed except those with order $3 \times 2 \times c$.

In order to verify the correctness of this method, we compared the two kinds of arrangements both with four SMRs. The error curve of the GSSMP rotation axis accuracy is shown in Fig. 16. The result shows that the RMS value of the uniform

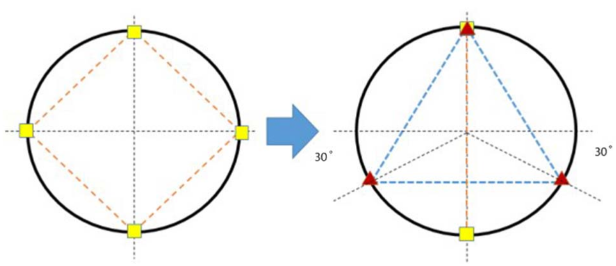

Fig. 12. Profile of the location of the SMRs.

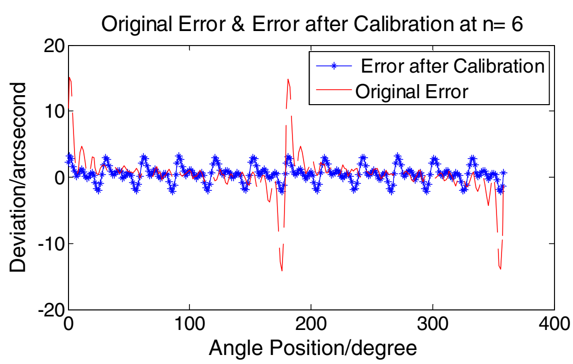

Fig. 13. Error series before and after averaging for new configuration.

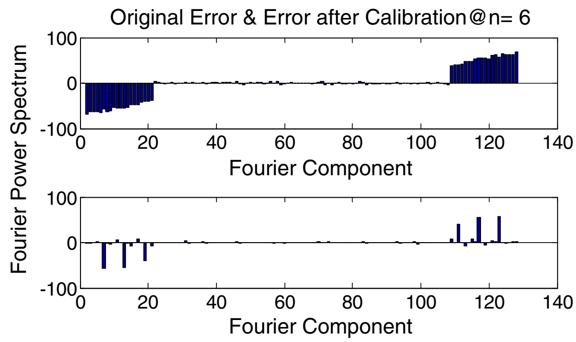

Fig. 14. Fourier components of the error before and after averaging for the new configuration.

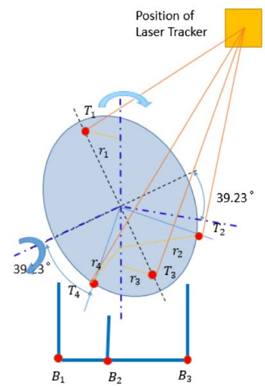

Fig. 15. Configuration of the testing plan for both tilt and rotation.

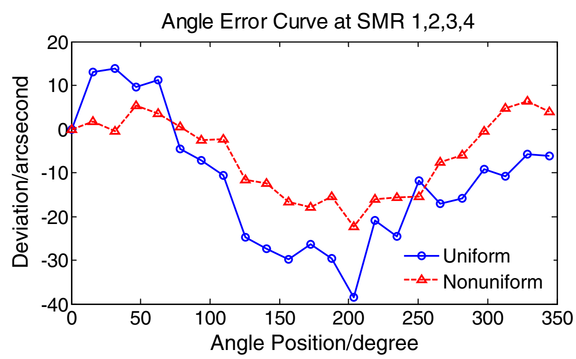

Fig. 16. Comparison result of the GSSMP rotation axis accuracy with different arrangement of the SMRs.

arrangement is 11.50″ (29.21 cm), and the nonuniform arrangement is 9.04″ (22.9616 cm). Thus, the accuracy of the measurement has been improved by 21.4%.

4. EXPERIMENT

As the GSSMP rotation axis has already been completely assembled, its accuracy can be measured. The rotation assembly has four reading heads with 32 bits each. For pointing and tracking, the M3S rotation range about the ECRS Z-axis shall be $\theta = +14°$ to $-28°$ for instruments on the $+X$ Nasmyth Platform and $\theta = +166°$ to $+208°$ for instruments on the $-X$ Nasmyth platform. Figure 17 shows a schematic diagram of the rotation range. The calibration range would be the same as in the actual work conditions [25].

As stated earlier, for the rotation axis, the step length is 1°. It is a good approximation to assume that the error is evenly distributed in this range. Figure 18 show the deviation of the encoder on the test and behavior of the ideal encoder. If the averaged error in the whole 1° step range met the requirements, we could ensure that arbitrary motion would also meet the requirements after calibration.

Here the resolution that is directly related to the minimum internal resolution of the encoder is $\tau_{\mathrm{resolution}}$. For both the rotation and tilt axes, the resolution is $\tau_{\mathrm{resolution}} = \frac{360°}{2^{32}} = 3 \times 10^{-4}$ arc sec and δ_{ti} is the error over a 1° step.

The number of electronic pulses n in the 1° step, which is theoretically equal to the grooves, is

$$n = \frac{1°}{\tau_{\mathrm{resolution}}} = 3314.$$

The requirement is a repeatable residual M3 rotation error (after telescope calibration) that is less than 5 arcsec RMS:

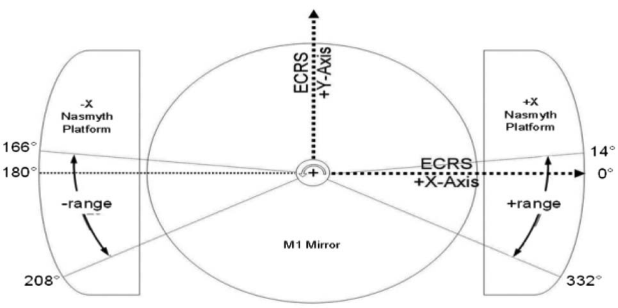

Fig. 17. Profile for the rotation range.

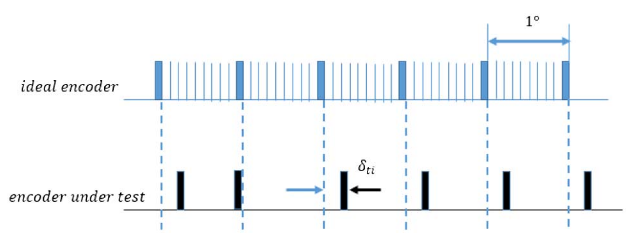

Fig. 18. Deviation of the encoder on the test and behavior of the ideal encoder.

$$\frac{K_n \delta_{\mathrm{ti}}}{n} \ll 5'',$$

where $K_n = 3-5$ is the safety coefficient.

5. CONCLUSIONS

An error analysis of the calibration is very necessary because tracking is the most important function of the GSSM. The unique motion of the GSSM has forced the positioning team to do their best to accomplish the goal. If the error was not sufficiently suppressed, this hard work would be wasted. In the error analysis, systematic errors were estimated by the standard bar method, while the drift and random errors can be distinguished using the correlation coefficient. The tests performed on the GSSMP yielded a systematic error of about 20 μm and a random error (averaging 15 min) of about 4 μm.

Funding. National Natural Science Foundation of China (NSFC) (11403022, 11673080); Youth Innovation Promotion Association of the Chinese Academy of Sciences (2016198).

Acknowledgment. The authors are very grateful to Dr. Zhao Hongchao and Dr. An Qichang for providing their valuable suggestions and help. We also thank the TMT group for use of their equipment and technology support.

REFERENCES

1. G. Z. Angeli, S. Roberts, and K. Vogiatzis, “Systems engineering for the preliminary design of the Thirty Meter Telescope,” Proc. SPIE **7017**, 701–704 (2008).
2. L. Stepp, “Thirty Meter Telescope project update,” Proc. SPIE **8444**, 84441G (2012).
3. F. Yang, G. J. Liu, and H. C. Zhao, “Stiffness allocation and analysis of TMT M3S,” Opt. Precis. Eng. **24**, 152–159 (2016).
4. H. C. Zhao, J. X. Zhang, F. Yang, Q. C. An, Y. Q. Su, and P. Guo, “Study of tilt axis bearing arrangement for M3S of TMT project,” Proc. SPIE **9280**, 92800M (2014).
5. J. Pazder, K. Vogiatzis, and G. Angeli, “Dome and mirror seeing estimates for the Thirty Meter Telescope,” Proc. SPIE **7017**, 70170R (2008).
6. B. Seo, C. Nissly, G. Angeli, B. Ellerbroek, J. Nelson, N. Sigrist, and M. Troy, “Analysis of normalized point source sensitivity as performance metric for large telescopes,” Appl. Opt. **48**, 5997–6007 (2009).
7. M. Troy, G. Chanan, S. Michaels, R. Bartos, G. Bothwell, R. Hein, M. Radin, J. Roberts, J. M. Rodgers, L. Sherr, B. Seo, and D. Zimmerman, “A conceptual design for the Thirty Meter Telescope alignment and phasing system,” Proc. SPIE **7012**, 70120Y (2008).
8. G. Chanan, M. Troy, and I. Crossfield, “Predicted measurement accuracy of the TMT alignment and phasing system,” TMT Project Communication TMT.CTR.PRE.07.007.REL01 (2007).
9. B. Seo, C. Nissly, M. Troy, G. Angeli, R. Bernier, L. Stepp, and E. Williams, “Estimation of normalized point-source sensitivity of segment surface specifications for extremely large telescopes,” Appl. Opt. **52**, 4111–4122 (2013).
10. W. N. Wang, Y. C. Su, and G. Y. Ren, “A study on dynamic character of laser tracker,” Acta Metrologic. Sin. **28**, 36–38 (2007).
11. H. B. Zhang, Q. H. Wan, S. J. Wang, H. Yu, and L. H. Liang, “Installation error control of dynamic measurement for small photoelectric encoder,” Opt. Precis. Eng. **24**, 1655–1660 (2016).
12. J. R. Lin, J. G. Zhu, H. L. Zhang, X. Y. Yang, and S. H. Ye, “Field evaluation of laser tracker angle measurement error,” Chin. J. Sci. Instrum. **33**, 463–468 (2012).

13. L. Q. Ma, J. H. Wang, T. Z. Cao, and Q. R. Li, “Calibration for angular error of laser tracker by small displacement,” Acta Metrologic. Sin. **30**, 76–78 (2009).
14. Y. Wang, Z. Xue, Y. Huang, and X. N. Wang, “Study on self-calibration angle encoder using simulation method,” Pro. SPIE **9903**, 99032O (2016).
15. R. D. Geckeler, A. Link, M. Krause, and C. Elster, “Capabilities and limitations of the self-calibration of angle encoders,” Meas. Sci. Technol. **25**, 055003 (2014).
16. B. Nissly, M. Seo, and M. Troy, “High-resolution optical modeling of the Thirty Meter Telescope for systematic performance trades,” Proc. SPIE **7017**, 70170U (2008).
17. B. Seo, C. Nissly, G. Angeli, D. MacMynowski, N. Sigrist, M. Troy, and E. Williams, “Investigation of primary mirror segment’s residual errors for the Thirty Meter Telescope,” Proc. SPIE **7427**, 74270F (2009).
18. D. Redding, *MACOS Manual (Modeling and Analysis for Controlled Optical Systems)* (NASA JPL, 1999), paper D9816.
19. T. L. Zobrist, J. H. Burge, and H. M. Martin, “Laser tracker surface measurements of the 8.4 m GMT primary mirror segment,” Proc. SPIE **7426**, 742613 (2009).
20. Y. Bao, X. W. Yi, Z. H. Li, Q. M. Chen, J. P. Li, X. D. Fan, and X. M. Zhang, “A digitally generated ultrafine optical frequency comb for spectral measurements with 0.01-pm resolution and 0.7-μs response time,” Light Sci. Appl. **4**, e300 (2015).
21. TMT Optics Group, “Design requirements document for tertiary mirror system (M3S),” TMT.OPT.DRD.07.006.REL29 (2012).
22. R. Probst, R. Wittekopf, M. Krause, H. Dangschat, and A. Ernst, “The new PTB angle comparator,” Meas. Sci. Technol. **9**, 1059–1066 (1998).
23. W. T. Estler, “Uncertainty analysis for angle calibrations using circle closure,” J. Res. Natl. Inst. Stand. Technol. **103**, 141–151 (1998).
24. T. Watanabe, H. Fujimoto, and T. Masuda, “Self-calibratable rotary encoder,” J. Phys. **13**, 240–245 (2005).
25. M. K. Cho, “Performance prediction of the TMT tertiary mirror, Ritchey–Chrétien design,” TMT.OPT.TEC.07.026.REL01 (2007).